The Meteoritical Society

Meteoritics & Planetary Science 43, Nr 12, 2015–2026 (2008)
Abstract available online at http://meteoritics.org

Laboratory investigations of marine impact events: Factors influencing crater formation and projectile survivability

D. J. MILNER[1*], E. C. BALDWIN[2], and M. J. BURCHELL[1]

[1]School for Physical Sciences, Ingram Building, University of Kent, Canterbury, Kent CT2 7NH, UK
[2]Department of Earth Sciences, University College London, Gower Street, London WC1E 6BT, UK
[*]Corresponding author. E-mail: djmilner26@hotmail.com

(Received 03 March 2008; revision accepted 07 January 2009)

Abstract–Given that the Earth's surface is covered in around two-thirds water, the majority of impact events should have occurred in marine environments. However, with the presence of a water layer, crater formation may be prohibited. Indeed, formation is greatly controlled by the water depth to projectile diameter ratio, as discussed in this paper. Previous work has shown that the underlying target material also influences crater formation (e.g., Gault and Sonett 1982; Baldwin et al. 2007). In addition to the above parameters we also show the influence of impact angle, impact velocity and projectile density for a variety of water depths on crater formation and projectile survivability. The limiting ratio of water depth to projectile diameter on cratering represents the point at which the projectile is significantly slowed by transit through the water layer to reduce the impact energy to that which prohibits cratering. We therefore study the velocity decay produced by a water layer using laboratory, analytical and numerical modelling techniques, and determine the peak pressures endured by the projectile. For an impact into a water depth five times the projectile diameter, the velocity of the projectile is found to be reduced to 26–32% its original value. For deep water impacts we find that up to 60% of the original mass of the projectile survives in an oblique impact, where survivability is defined as the solid or melted mass fraction of the projectile that could be collected after impact.

INTRODUCTION

Impact cratering is a ubiquitous geological process throughout the Solar System, to which the Earth is just as vulnerable as any other planetary body. The current surface topography of the Earth implies a heavy bias towards marine environments, with approximately 60% of the Earth's surface being covered by deep water. Assuming this is a distribution which has been stable for considerable time it is reasonable to assume that the majority of impacts upon the Earth have occurred in marine environments. Of the 175 impact structures that have been discovered upon the Earth only 33 are recognized as having formed in a marine environment (Gersonde and Deutsch 2000; Ormö and Lindstrom 2000; Gersonde et al. 2002; Allen and Stewart 2003; Dypvik and Jansa 2003). Furthermore, of these, very few are at present still fully in a marine environment (e.g., one example is the 40 km wide Mjølnir impact crater in the Barents Sea [e.g., Tsikalas et al. 1999; Dypvik et al. 2003]), with most now being located on land due to changes in sea level. This lack of marine impact structures may initially seem surprising, but can easily be explained by a number of factors, the most important being the depth of the water layer, discussed later. Second order factors include a general lack of detailed topography of the ocean floor and the deep sea basement having a finite lifetime of 150–200 million years due to plate subduction. In addition, any craters which do remain may be heavily eroded and infilled with sedimentary layers. Furthermore, as an inevitable consequence of water being present at the impact site, and also due to the repetitive process of resurge into the crater as the water level regains equilibrium, the crater rim will become heavily eroded. It should also be noted that dependant upon the water depth the elevated rim may not be developed at all due to the effects of a layered target (Ormö and Lindstrom 2000). As mentioned previously, the depth of the ocean plays an important role in determining the efficiency of cratering at the ocean floor, by causing significant disruption to an asteroid before it has the opportunity to strike the basement rock. The water depth at which a crater no longer forms is influenced by the underlying target material, with lose unconsolidated strata such as sand requiring a greater depth of water to prevent cratering than a consolidated basement rock, as demonstrated through laboratory experiments by Gault and Sonnet (1982) and

Fig. 1. The University of Kent two-stage light gas gun (LGG). The gun is 5 m in length and in this image fires from bottom left to top right.

Baldwin et al. (2007), respectively. In these experiments, Gault and Sonnet (1982) demonstrated that a water depth (H) of twenty times the projectile diameter (*d*) was required to prevent cratering in sand targets, compared with Baldwin et al. (2007) who showed that this critical H/*d* ratio was 11.6 ± 0.5 and 12.7 ± 0.6 for unsaturated and saturated sandstone targets, respectively, for planar impact events at ~5 km s^{-1}. For impact experiments into water overlying granite, we show the H/*d* ratio is between 7.5 and 10; this is described in more detail later in this paper, but fits with the trend that an increasingly stronger basement rock requires less overlying water to protect it from cratering. The critical depth at which a sea floor crater is formed in planetary scale events has been investigated numerically (e.g., Shuvalov and Trubetskaya 2007; Ormö et al 2002), for example, in a discussion on the effects of a marine impact on shock metamorphism of the ocean floor, Artemieva and Shuvalov (2002) show that oceanic depths twice that of the projectile diameter begin to influence crater formation, while for water depths four times the projectile diameter a sea-floor crater is almost non-existent, for typical planetary impact velocities of 15–40 km s^{-1}. Whether in the lab or at planetary scale, the critical H/*d* value signifies the point at which the projectile has been decelerated significantly during transit through the water layer, resulting in a low deposition of energy at the basement rock not sufficient to cause crater excavation. This paper will focus on the effect of water depth on crater morphology in granite, and will look in detail at the decay in velocity and pressure within the projectile as it traverses the water column. We also investigate the effect of projectile velocity and impact angle on crater morphology in granite with an overlying water layer.

Previous laboratory work has shown already that some proportion of the projectile can survive a lab scale deep water impact event. For example, Gault and Sonett (1982) demonstrate that for an impact at 2.7 km s^{-1}, lens like disks of aluminium projectile containing 95–98% of their pre-impact mass survived, decreasing to 20% for a 4.4 km s^{-1} impact and 0% recovered for impacts at 5.6 km s^{-1}. In recent work, Milner et al (2006) showed that up to 10% of the original mass of a shale projectile survives a 5 km s^{-1} laboratory scale impact event into water layers overlying a crystalline basement rock and Baldwin et al. (2007) showed that 25% of the mass of a stainless projectile survived impact into water overlying sandstone. We discuss the role of a water layer, and additional parameters such as impact velocity, angle and projectile density, on the fate of the projectile.

METHODOLOGY

All impact experiments use the University of Kent's two-stage light gas gun (LGG; for details of its operation refer to Burchell et al. 1999). The LGG (Fig. 1) is capable of accelerating millimeter scale projectiles to velocities of up to approximately 8 km s^{-1}. The gun, which fires horizontally, utilizes a water target holder for the work reported here. This holds a thin walled plastic bag of water flat against an underlying basement rock, with the capability to adjust the water depth from shot to shot as required (Fig. 2). Extensive test shots showed that the thin walls of the plastic bag had negligible influence on the resulting crater morphology. For the purpose of the present paper, we use the LGG to accelerate 1 mm diameter stainless steel 420 (420 refers to the grade and hence strength of the steel used in the experiment) projectiles to velocities of approximately 5 km s^{-1} (speed measured in each

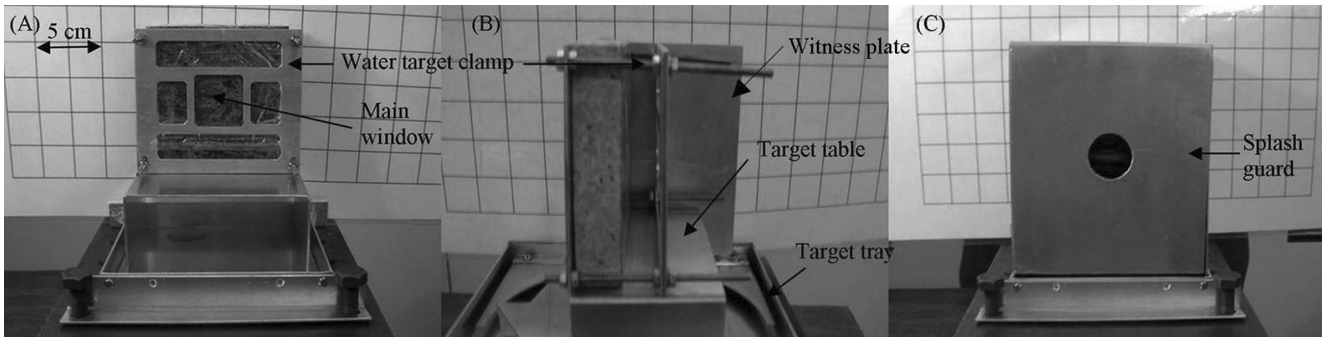

Fig. 2. Series of images showing the water target configuration. a) Face view of the water target. b) Side view of water table and clamp. c) Face view of water target with splash guard. The target holder comprises a water tray used to contain the water after the impact, a target table where the rock target is placed, a water target clamp which holds the water layer in position, and the splash guard which is placed over the target to minimize the amount of water and projectile that can escape during the impact. The target clamp has five windows, the largest of which is the primary target window through which the projectile passes. A witness plate is shown in the centre image, which is used to record the number of craters that result from ricochet of the projectile off the top of the water column.

Table 1. Effect of water depth on crater dimensions in granite, for planar impacts of 1 mm diameter stainless steel 420 projectiles. All measurements for the depth and diameter quoted in this paper are to an accuracy of ±0.05 mm and all measurements for volume are to within 0.015 cm^3. (The maximum difference between repeated measurements for volume).

Water depth (mm)	Impact velocity (km s^{-1})	Crater diameter (mm)	Crater depth (mm)	Crater volume (cm^3)
0	5.3	30	4.4	0.73
1	5.32	19	3.64	0.4
3	5.23	13	2.14	0.07
5	5.49	8.5	0.74	0.02
7.5	5.15	2.19	0.23	0
10	5.28	No crater	No crater	No crater
25	5.23	No crater	No crater	No crater
40	5.54	No crater	No crater	No crater

shot to better than typically 1%) into varying depth water layers overlaying a granite basement rock. Granite was chosen for its similar strength properties to the basaltic ocean floor, however it is worth noting that the "ocean floor" used in the experiments will have a greater strength than the true ocean floor given that strength decreases with increasing scale size (Housen and Holsapple 1999). The results, where appropriate, are compared to previously published work which focused on the effect of a water layer on crater morphology in saturated and unsaturated sandstone (Baldwin et al. 2007). For all experiments, the crater diameter, depth and volume were analyzed. The crater diameter was determined by using digital callipers to measure the diameter at a number of cross sections. Given the small-scale nature of the impact craters produced in the lab, it is very difficult to separate the effects of spallation from the true impact crater. Through our own estimates we have found that the measured diameters are up to 25% greater than the estimated transient crater diameters (Baldwin et al. 2007). For the purpose of this paper, and to compare with the work published in Baldwin et al. (2007), we discuss the measured (spallation) diameter. A 2D profilometer system was used to measure the depth below the pre-impact surface at 1 mm increments over a cross section of the crater. To determine the volume of the crater cavity we used uniform, fine-grained spherical glass beads with diameters of a few micrometers. The beads were poured into the crater until the cavity was uniformly filled. The mass of beads required to fill the cavity was converted to volume by using a predefined calibration graph (Milner 2007). It was also possible to retrieve fragments of the projectile after the impact event. The material excavated from the crater was filtered using distilled water and Whatman grade 1 filter paper. The filter paper was then dried using an industrial strength hot air blower and the steel (magnetic) projectile fragments were separated from any rock fragments using a strong magnet, placed in a separate container, and weighed using a fine torsion microbalance (sensitivity ± 0.5 ng). In the first shot program we focus on the effect of a water layer on crater depth/diameter in granite and sandstone. We also investigate the effect of impact angle, impact velocity and projectile density on crater formation in a granite target with an overlying water layer. In the second shot program we investigate the effect of a water layer on projectile survivability, as well as the influence of projectile velocity, density and angle of impact for varied water depths.

RESULTS

Shot Program 1: Crater Morphology

Effect of Water Depth on Crater Morphology

In this shot program, the influence of a water layer of varying depth (0–40 mm) on crater diameter, depth and volume is investigated (Table 1 and Fig. 3). It can clearly be seen that for a granite basement rock, as the water depth increases there is an exponential decrease in all crater dimensions. For our craters in sandstone, described in more detail in Baldwin

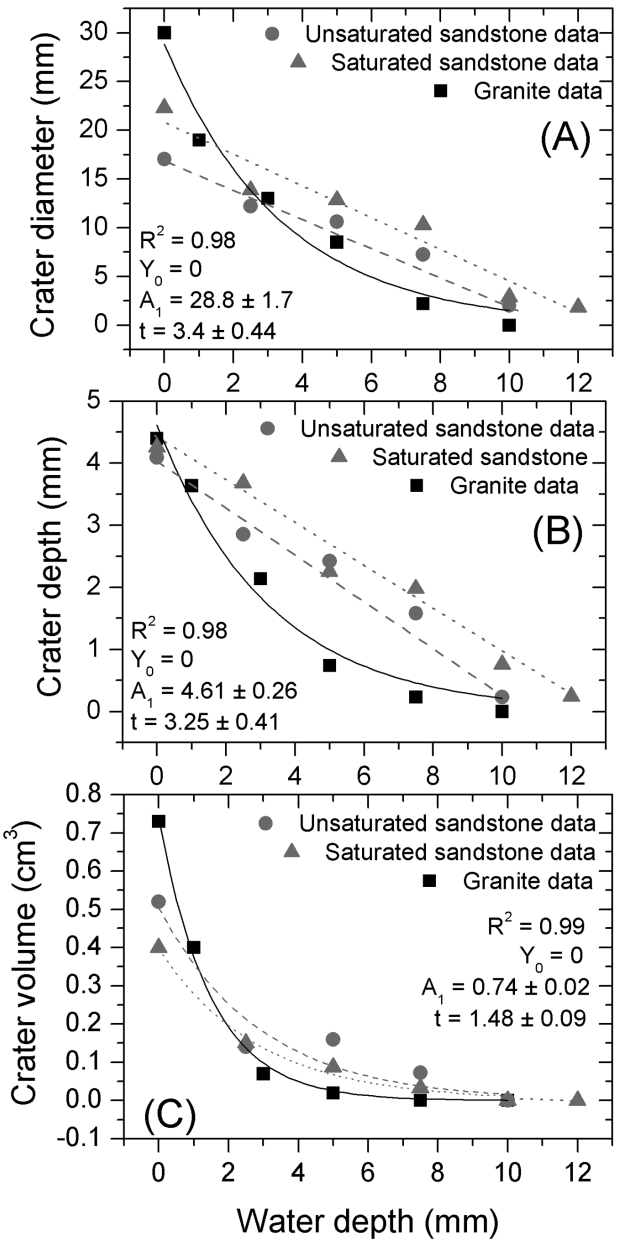

Fig. 3. Comparison of crater (a) diameter, (b) depth, and (c) volume in granite (data in Table 1) compared with previously published work in sandstone. For sandstone the average impact velocity was approximately 5 km s^{-1}, similar to that of the data in Table 1. All impacts were planar and used 1mm diameter stainless steel projectiles. (For data please refer to Baldwin et al. 2007).

et al. (2007), we find a linear decrease in dimensions. Since the lab conditions for the two rock types were identical, we can only presume that the different properties of the target rocks are causing this difference, for example differences in material strength, density and/or porosity, the effects of which cannot be separated in this study. For craters into granite the results imply that the presence of even shallow marine environments quickly influences the impact process. Indeed, a crater approximately 30 times the diameter of the projectile can be created in the absence of water, but as the water depth becomes equal to the projectile diameter the crater diameter is decreased by one third. It can also be seen that as the water approaches a depth (H) greater than ten times the projectile diameter (d) no crater forms on the ocean floor. For saturated and unsaturated sandstone the equivalent values were found to be 12.7 ± 0.6 and 11.6 ± 0.5, respectively. Although these results are very similar, considering also the experimental results of Gault and Sonett (1982) who showed that a water depth greater than 20 times the projectile diameter is required to prevent cratering in sand, the data for all three basement materials follows the rule that the weaker the material, the deeper the water required to prevent cratering.

Effect of Impact Velocity on Crater Morphology

A range of impact velocities between 1 and 7 km s^{-1} were investigated for normal incidence impacts (Table 2 and Fig. 4) into water depths up to five times the projectile diameter. This ratio was selected in order to still allow a crater to form in the basement rock, but also allowing the projectile to interact with the water column. Figure 4 shows an exponential decrease in the rate that the crater diameter increases with increasing impact velocity, for all water depths. This implies that at a certain impact velocity the crater diameter would fail to increase further, for our 1 mm diameter projectiles.

Effect of Impact Angle on Crater Morphology

For impact events where the water column is kept constant but the angle of impact is increased from zero degrees (normal incidence), the crater diameter is expected to decrease due to the water depth in the line of sight of the projectile increasing, hence slowing the projectile further and resulting in a lower fraction of energy being deposited at the basement rock. Indeed, Fig. 5 (and Table 3) shows that for impact angles of 45, 60, and 70 degrees from the vertical, if the crater diameter is plotted against water depth normalized to the impact angle, the oblique impact events produce craters that follow a similar trend to the normal incidence craters. The craters were also observed to remain circular, consistent with other experiments (e.g., Burchell and Whitehorn 2003 and references therein) that demonstrated oblique craters forming only at impact angles of 85 degrees. We therefore investigate varying impact angles into a constant column length of 5 mm (i.e., the water depth is varied to ensure this 5 mm column length is maintained) so that impact angle is the only variable. Figure 6 shows a clear trend that as the impact angle increases from the normal, the diameter of the craters produced are reduced linearly. This can be explained by the fact that as the impact angle becomes more oblique the peak shock pressures produced in the isobaric core of the target (and also in the projectile, see later) are reduced, since the peak shock pressure is governed by the vertical component of the projectiles velocity, $V\cos\theta$

Table 2. Varied impact velocities at varied water depths using 1 mm diameter stainless steel 420 projectiles, and corresponding crater diameter in granite. This data is displayed in Fig. 4.

Water depth (mm)	Impact velocity (km s^{-1})	Crater diameter (mm)
0	1.019	5
0	2.89	14
0	4.99	20
0	6.49	24
1	1.09	4.295
1	3.02	10.13
1	5.38	16.4
1	7.07	18
2	1.37	6.43
2	2.02	6.44
2	3	11.97
2	4.61	13.48
2	6.01	13.69
2	7.14	17.27
5	1.02	0.1
5	2.89	10.67
5	5.01	6.65
5	5.06	7.76
5	7.22	7.38
10	1.03	No crater
10	2.89	No crater
10	5.03	No crater
10	7.07	No crater

Table 3. Change in crater diameters in granite for different impact angles and water depths. This data is shown in Fig. 5.

Water depth (mm)	Impact angle (degrees)	Impact velocity (km s^{-1})	Crater diameter (mm)
0	45	5.36	24
5	45	5.37	0.5
3	45	5.23	11
1.5	60	5.31	12
1.5	75	5.294	4

Table 4. Percentage of surviving projectile expressed as mass of original projectile mass collected after impacts into granite with 0–40 mm overlying water.

Water depth (mm)	Impact velocity (km s^{-1})	Percentage of surviving projectile (%)
0	5.3	2.4
1	5.32	2.9
3	5.23	15
5	5.49	28
7.5	5.15	22
10	5.28	30
25	5.23	23
40	5.54	24

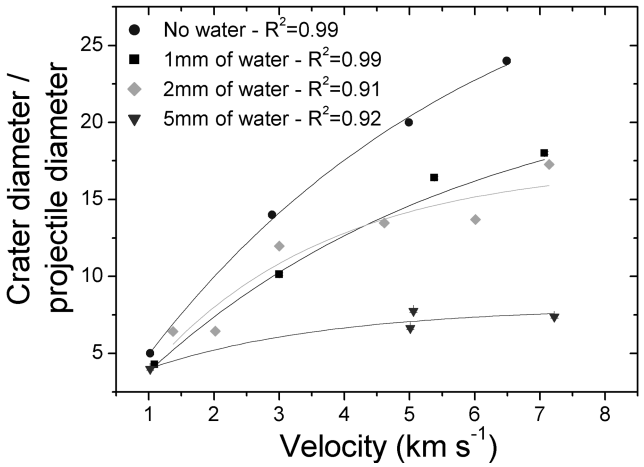

Fig. 4. Change in crater diameter in granite as the impact velocity increases for water depths between 0 and 5 mm All impacts were planar and used 1 mm diameter stainless steel 420 projectiles All fits use first order exponential decay plots ($Y = Y_o + e^{(-x/t)}$).

(Pierazzo and Melosh 2000a, 2000b). So, as the impact angle increases, the vertical component of the impact velocity is reduced, thus reducing the energy delivered to the target.

Shot Program 2: Projectile Survivability

Asteroid impact events into water are conducive to projectile survival (Shuvalov and Trubetskaya 2007). Hence, in the second shot program we investigate the effect of impact angle, impact velocity and projectile density into varied water depths on the fate of projectile. It is important to note that when the surviving fraction of projectile is discussed it refers to the projectile which remained unmelted or melted in the impact event, and so can be collected, and not any material that vaporized.

Effect of Water Depth on Projectile Survivability

The results for the surviving fraction of projectile can be seen in Table 4 and Fig. 7. It can be seen that as the water depth increases the percentage of surviving projectile fragments increases initially at an exponential rate. This implies that at shallow water depths (equivalent to the diameter of the projectile) the water layer does not significantly affect the surviving fraction. However, as the water depth becomes larger than the projectile diameter the percentage of surviving projectile rapidly increases. This happens until the water depth reaches a value at which no crater forms in the basement rock, approximately ten times the projectile diameter for a stainless steel projectile impacting into water layers overlying granite. At this value, the surviving projectile mass reaches a maximum and remains constant irrespective of increasing water depth, indicating the strong influence that interaction with the basement rock has on determining the fate of the projectile.

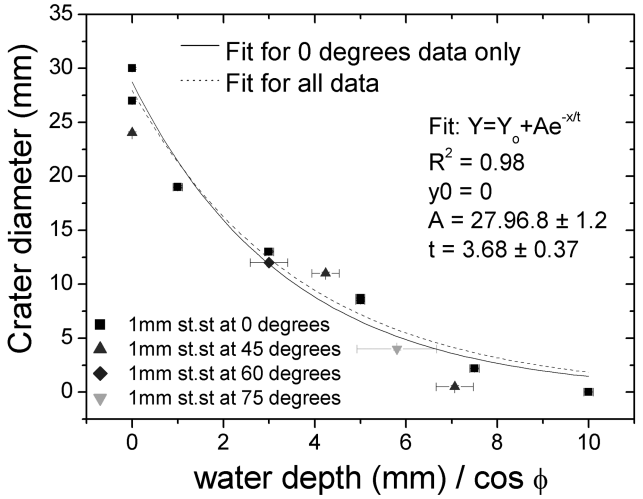

Fig. 5. Change in crater diameter as the water depth and impact angle increases for 1 mm diameter stainless steel 420 projectiles impacting between 5.25–5.37 km s^{-1}. The water depth is normalized to the impact angle so that the impacts are plotted dependent upon the column length of water the projectile traverses and not the water depth.

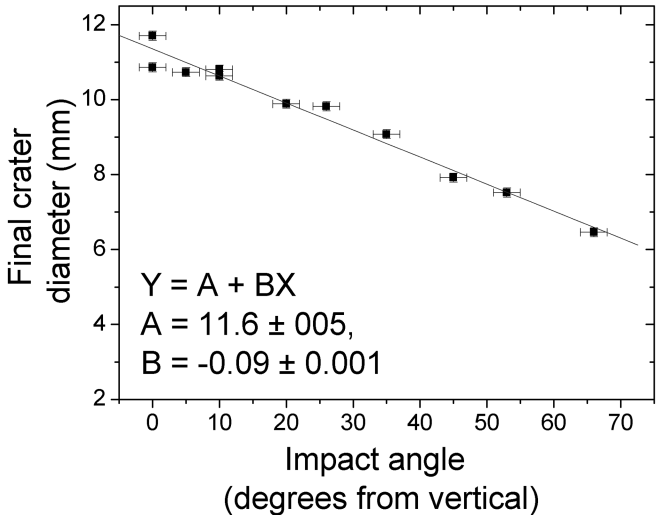

Fig. 6. Change in crater diameter as the impact angle and water depth vary to maintain a constant column length. All impacts use 1 mm diameter stainless steel 420 projectiles impacting at approximately 5 km s^{-1}, $R^2 = 0.96$.

Table 5. Percentage of surviving projectile for impacts into deep water (15 mm) at different impact angles for 1 mm diameter stainless steel 420 projectiles impacting between 5.0–5.39 km s^{-1}. The column length that the projectile traverses thus increases with increasing impact angle.

Impact angle (degrees)	Column length (mm)	Impact velocity (km s^{-1})	Percentage of surviving projectile (%)
0	15	5.39	38.3
5	15.06	5.34	46.1
10	15.23	5.28	57.8
25	16.55	5.28	54.9
45	21.2	5.39	56.2
45	21.2	5.00	56
55	26.15	5.29	44.4
55	26.15	5.09	37.2
65	35.49	5.19	47.2
65	35.49	5.04	46.3
70	43.85	5.12	32.88
75	57.96	5.26	34
75	57.96	5.15	17.9

Effect of Impact Velocity on Projectile Survivability

In this shot program the impact velocity of the projectile was varied between 1 and 7 km s^{-1}, representing the optimal range of operation of the light gas gun, into water depths of 2, 5 and 10 mm, to represent the cases where water has shown to have no, some or little effect on projectile survivability or crater formation in previous experiments. It is clear from Fig. 8 that irrespective of water depth, an increased impact velocity causes an exponential decay in the surviving projectile mass. For the range of velocities investigated here this curve never reaches zero. Ignoring issues of scale/size,

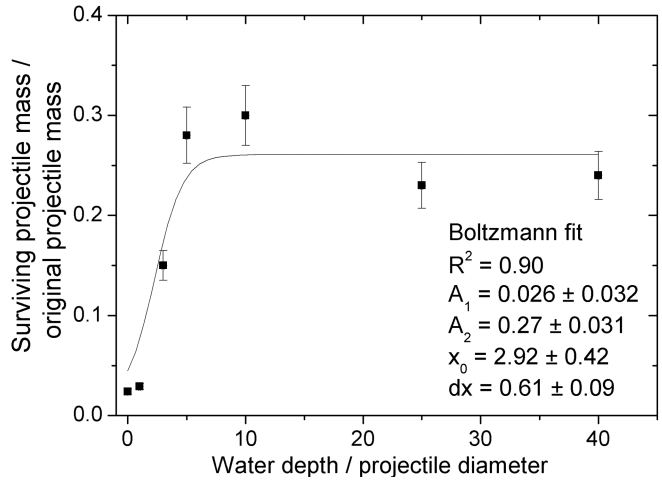

Fig. 7. Surviving projectile fraction as water depth increases for 1 mm diameter stainless steel 420 projectiles impacting between 5.23–5.54 km s^{-1}. The data has been plotted using a Boltzmann fit expressed by $Y = [(A_1 - A_2)/(1 + e[(x - x_0)/dx])] + A2$.

this would imply that even at planetary scale impact velocities (approximately 25 km s^{-1}), we could still expect to find around 30% of the projectile surviving the impact. Vaporization, however, will occur at these higher velocities, significantly reducing the surviving mass. Furthermore, the size distribution of the fragments (not investigated here) may differ greatly at different scales, given that the overall strengths of the objects involved decrease with increasing scale size (Housen and Holsapple 1999).

Effect of Impact Angle on Projectile Survivability

In testing the fate of the projectile at oblique angles, a water depth of 15 mm was selected to prevent any basement

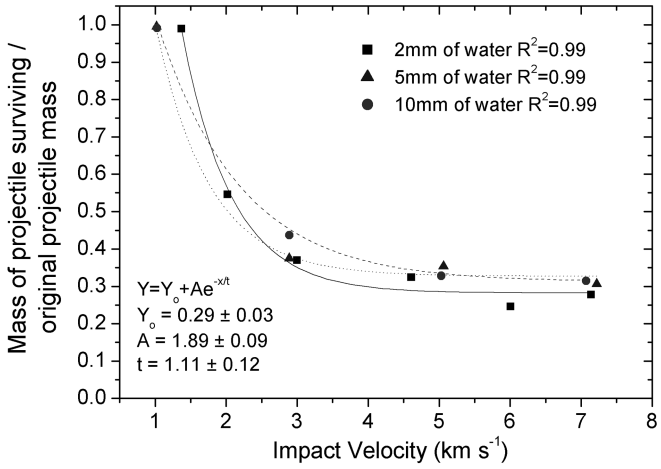

Fig. 8. Surviving projectile fraction as impact velocity increases, for the planar impact of 1 mm diameter stainless steel 420 projectiles, at various water depths. The data are fit to the exponential decay displayed on the graph. The R^2 coefficients for each line are shown on the graph and indicate that the lines represent the data well. The error bars associated with the data can not be seen as they are so small. As the data points and lines overlap each other the fit data shown on the figure represents that for a line fitted through all the data points.

Table 6. Density (ρ), C, and S values used in the LE calculations.

Material	ρ, (kg m^{-3})	C, (m s^{-1})	S
Stainless steel	7800	4610	1.73
Water	1000	1674	1.92
Granite	2630	3680	1.24

rock/projectile interaction. It can be seen that as the impact angle is increased from the vertical, the percentage of surviving projectile dramatically increases to a peak of approximately 60% for impact angles of 30–35 degrees from the vertical, decreasing again for the most oblique impact angles (Table 5 and Fig. 9). Pierazzo and Melosh (2000a, 2000b) show that for planetary scale models, the peak shock pressures in both the projectile and the target are greatly reduced as the impact angle increases towards the horizontal. As a consequence of this, the percentage of the projectile which is melted and vaporized during the impact also decreases. However, even at oblique angles (up to 60 degrees from the vertical) the majority of the projectile and target are still exposed to peak shock pressures that cause significant melting and vaporization of the projectile, for the modelled impact of a dunite projectile impacting the Earth's surface at 25 km s^{-1}. Indeed for a vertical impact, pressures greater than 500 GPa are reached in the projectile, which decrease linearly to around 100 GPa for an impact 15 degrees from the horizontal (Pierazzo and Melosh 2000b). Of course, at these large scales, the strength of the target rock will be considerably less than that at a lab scale, and the strength of the rock decreases as the loading duration increases (Housen

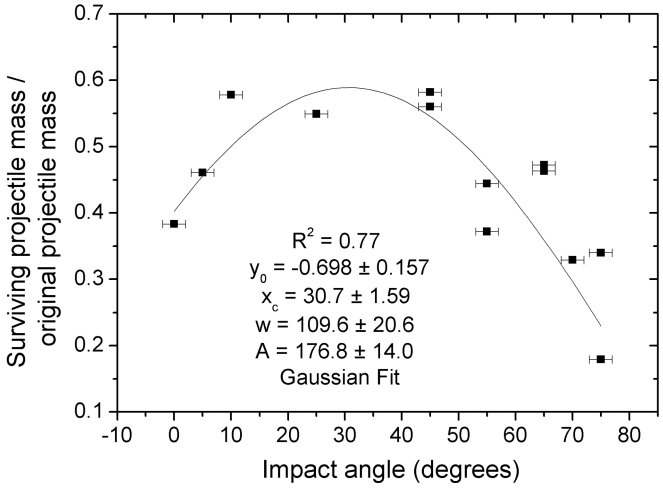

Fig. 9. Surviving projectile fraction as impact angle increases from the vertical for impacts into deep water (15 mm) for 1 mm diameter stainless steel 420 projectiles impacting between 5.25–5.37 km s^{-1}. The data is fit with a Gaussian fit given by: $Y = Y_0 + \{(A/\{W[(\pi/2)^{1/2}]\})e[-2(X-X_c)^2/W^2]\}$.

and Holsapple 1999). It is therefore unsurprising that a large amount of the projectile can be recovered in our experiments into deep water, since the lab specimens will be stronger than their planetary-scale counterparts. We determine the peak shock pressures, P_O, endured by the lab scale projectiles using the late stage effective energy technique (LE) of Mizutani et al. (1990), given by:

$$P_0 = \frac{1}{2}\,\xi\,\rho_{ot}\,c_t^2\left(1+\frac{1}{2}\,S\xi\frac{v}{c_t}\right)\left(\frac{v}{c_t}\right) \quad (1)$$

where c_t and s are the target material parameters from the shock wave speed equation of state, ρ_{ot} is the initial density of the target; v is the impact velocity; and ξ is a parameter related to the shock impedance matching (i.e., the peak pressures which occur in the projectile and the target at the same time) defined by:

$$\xi \approx 2\Big/\left\{1+\left(\frac{\rho_{ot}c_t}{\rho_{op}c_p}\right)\right\} \quad (2)$$

where the subscripts t and p refer the target and projectile parameters, respectively. If the target and the projectile are the same material, then ξ is equal to 1 and ξ can be neglected from Equation 1. Data used in these calculations are presented in Table 6. Using this equation it is possible to factor in the effect of a varied angle by taking the velocity to be the vertical component of the projectile's velocity. It should be recalled however, that a single measure of peak pressure such as this applies only to a small region of the projectile; the rest of the projectile is shocked to lower peak pressures (Crawford et al. 2008). For the case of a 1 mm stainless steel projectile impacting a granite target at

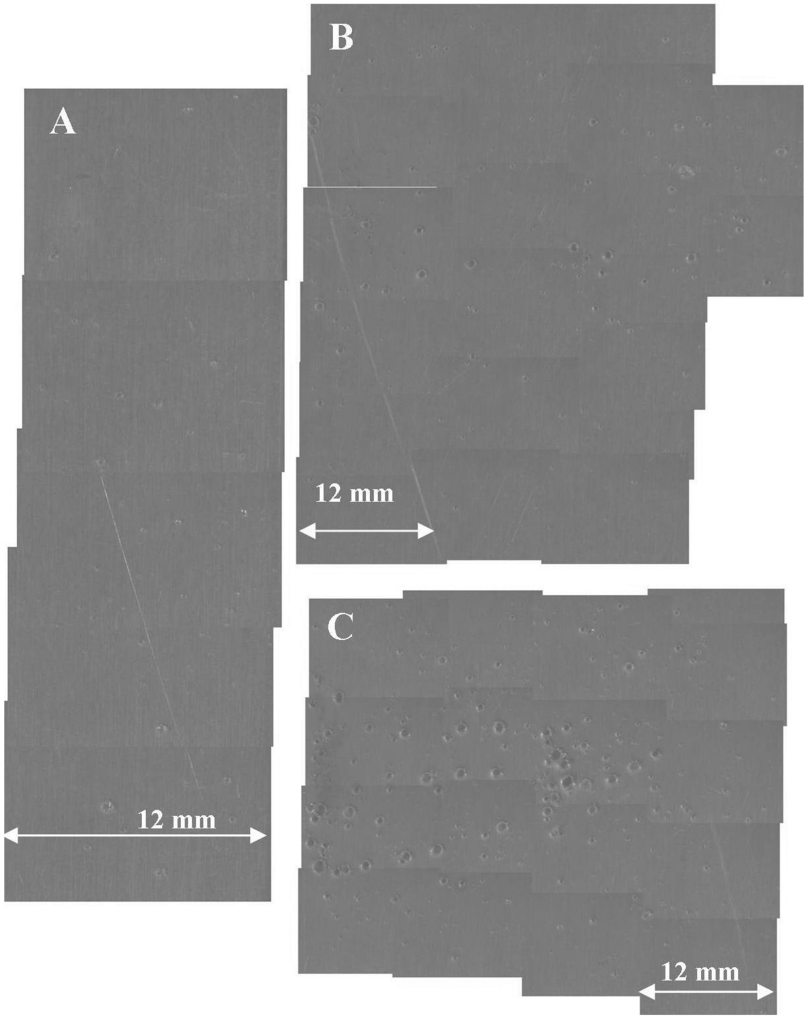

Fig. 10. Mosaics of the witness plates after impacts at different angles, revealing the extent of ricochet for impacts at (a) 65 degrees, (b) 70 degrees and (c) 75 degrees. The witness plate was attached perpendicular to the end of the target holder (in the downrange direction), with the far left hand side of the plates shown above inline with the pre-impact water surface. As the impact angle increases, the size of the angle over which the ricochet occurs increases, as does the number of downrange impacts.

5 km s^{-1} with no water layer present, a vertical impact produces peak shock pressures of 89 GPa decreasing to 13 GPa for an impact at 85 degrees from the vertical. Although these shock pressures are far lower than the planetary scale impacts it is clear that they are still considerably greater than the strength of the stainless steel projectile (520 MPa; as determined in the laboratory) and hence we would expect the projectile to be heavily fragmented. Furthermore, the pressure required for melting is estimated to be ~220 GPa (comparable to the melting pressure of iron given by Melosh [1989]), therefore we should expect high survivability rates. In addition, the presence of a water layer will slow the projectile before impacting the basement rock and hence the peak shock pressures will be reduced further still. Indeed, an LE calculation for the scenario of our projectile impacting into deep water yields a maximum peak pressure of 52 GPa for planar impact. However, our results imply that survivability is favoured for angles between 25 and 45 degrees, with survivability decreasing with the most oblique angles. The corresponding peak pressure as calculated by the LE technique for a 45 degree impact into deep water is 27 GPa.

For highly oblique impact angles, we note that the projectile can undergo some form of ricochet and skip off the water layer whilst maintaining a significant proportion of its impact velocity, impacting further downrange of the initial impact point, therefore striking the target casing in our experimental setup and possibly vaporize/melting upon contact with the solid surface, making our final surviving fraction found in the crater considerable reduced from the peak value. We therefore recorded the craters on the witness plate, which was attached perpendicular to the water layer and downrange of the target (labelled in Fig. 2). For impacts at 45 degrees and 55 degrees there were no craters or even

blemishes upon the witness plate, indicating that no ricochet is occurring at this angle (Fig. 10a). However, as the impact angle reaches 65 degrees the witness plate is becoming obviously cratered (Fig. 10b), and becoming even more heavily cratered for more oblique impacts, suggesting that as the impact angle increases from planar (0 degrees) to horizontal (90 degrees), the reflected projectile fragments into more pieces. Moreover, it is observed for the 75 degree impact that one of the fragments punctures a hole through the plate (Fig. 10c). This has two possible implications. The first is that the size of the largest fragment is larger than at the previous two angles, increasing its impact energy and hence allowing it to puncture a hole in the plate. However, given that the plate is covered in more craters than at lower angles, this suggests that there are an increasing number of smaller projectile fragments. More likely though, is that the fastest moving fragment maintains a greater proportion of the projectile's initial velocity hence providing larger impact energies than in an increasingly planar impact. When the impact angle becomes more oblique, the horizontal component of the projectile's velocity is increased, and this horizontal component becomes the vertical component of the impact on a perpendicular witness plate and hence is responsible for the impact energy and resultant target deformation. We also note that as the impact angle becomes more oblique, the angle of ricochet of the fragments with the greatest energy at impact is increased from the horizontal. For example, for the 65 degree shot, the heaviest cratering occurs between 0–12 mm of the water level, corresponding to a possible angular range of 0–12 degrees, as determined through simple trigonometry. However, for the 75 degree impact the heaviest cratering occurs around 24 mm away from the water level (i.e., $\theta = 22$ degrees), and to 40 mm (42 degrees) for the 75 degree impact. Of course, at a planetary scale impact into an ocean there will be no witness plate to 'capture' a potentially ricocheted projectile, hence our results are biased to laboratory conditions only. At larger scales we can conjecture that the ricocheted projectile fragment (or even whole projectile) will re-impact the ocean downstream of the initial point of contact at a reduced velocity. Since 45 degrees is predicted as the most common impact angle upon the Earth (Shoemaker 1962), and our lab experiments show this angle to yield some of the highest survivability rates, the survivability of meteoritic material in the Earth's oceans is surely favored.

Effect of Projectile Density on Projectile Survivability

For this shot program various projectile materials were impacted into water depths 15 times the projectile diameter to ensure no cratering in the basement rock occurred and hence a maximum surviving fraction at normal incidence was achieved. Figure 11 shows a linear relationship between the projectile density and the surviving fraction. It is interesting to note that in some cases various projectiles of approximately the same density, but different strengths were used. For example, copper and stainless steel 420 projectiles have similar densities but very different compressive strengths of 220 MPa and 520 MPa, respectively. Indeed, copper has the higher density but the lower strength. The lab experiments show that no significant difference in projectile survivability was observed between these two materials, suggesting the density of the projectile plays a greater role in determining the fate of the projectile than material strength.

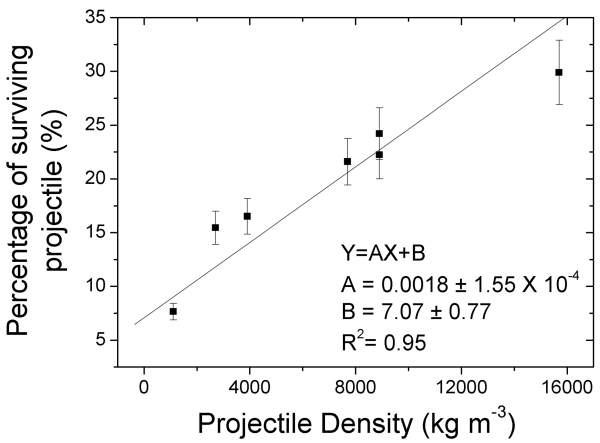

Fig. 11. Surviving projectile fraction as projectile density increases, for varied projectile materials, impacting at approximately 5 km s^{-1} into 15 mm deep water layers.

ANALYTICAL INVESTIGATION

Velocity Decay in the Projectile

The velocity decay of the projectile as it traverses a water layer was calculated using 1) experimental data, 2) the Supersonic Drag Equation (described in detail in O'Keefe and Ahrens 1982), 3) AUTODYN numerical models. A brief description of each method follows:

1. The experiments were used to study the velocity decay of the projectiles at the basement rock after traversing the water layer. This velocity was determined by using the data for impacts of 1-millimeter-diameter stainless steel projectiles over a range of velocities directly into a granite rock with no water layer. The transient crater diameter produced in the basement rock after the experiments with water layers was then compared to the results versus velocity without water present and an equivalent cratering velocity obtained. It is important to note that while this method provides a simple way of calculating the velocities at the basement rock in the absence of any high-speed cameras, there is the potential for underestimating the velocities since the projectile will become progressively fragmented and dispersed for deeper water impacts.
2. The supersonic drag (SSD) approximation allows an analytical calculation of projectile speed as it moves

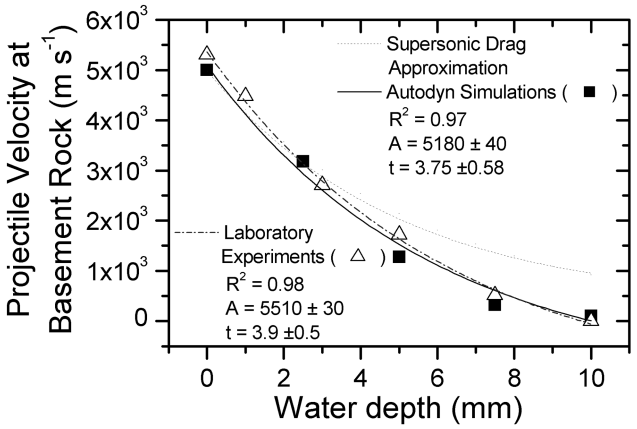

Fig. 12. Final velocity of the projectile at the ocean-target interface (point of impact with basement rock) as the water depth increases for experiments, AUTODYN simulations, and the supersonic drag approximation of a 1 mm diameter stainless steel 420 projectile. The lines are fitted to an exponential decay curve.

through a fluid medium, as described by O'Keefe and Ahrens (1982):

$$v(t) = \frac{1}{3(\rho_w/4r\rho_p)tc_d + 1/v_o}, \quad (3)$$

where $v(t)$ is the velocity at time t, ρ_w is the density of the water column, r is the radius of the projectile, ρ_p is the density of the projectile, c_d is the drag coefficient for a rigid sphere (0.877) and v_o is the initial impactor velocity at $t = 0$.

3. The commercially available numerical code AUTODYN-2D was used to simulate the laboratory experiments using the Smooth Particle Hydrodynamics (SPH) solver. Many materials are predefined in the AUTODYN material library, with a choice of equations of state (EOS), strength and failure models. In general, for the simulations defined here, the shock EOS was used to describe the stainless steel projectile, and the Tillotson EOS to describe granite (values of which are given in Melosh [1989], p. 232).

The geometry of the laboratory experiments were replicated in the simulations with a resolution of 20 SPH particles per projectile diameter. Tracer particles (or gauge points as they are called in AUTODYN) were distributed throughout the projectile and the target in order to record information about the velocity decay of the projectile during its traverse through the water layer. The velocity values in the projectile are taken at the point the projectile reaches the pre-impact ocean-target interface, to ensure consistency between the simulations. Cratering begins before the projectile strikes the surface as a result of the initial shock wave created in the impact event that travels ahead of the projectile, compressing the target basement rock. The decay in projectile velocity for both the models and the experiments were determined and compared (Table 7 and Fig. 12), along with the decay in projectile velocity determined by the supersonic drag approximation (SSD). The experimental data and hydrocode simulations provide very similar results showing consistency between the models and experiments. The SSD agrees well with the experimental results and numerical models for low water depths. At higher water depths (>3 mm) this analytical technique appears to deviate from the experimentally and numerically derived values. One consideration is that the equation assumes a constantly rigid, undisrupted sphere, whereas in reality, the projectile will become compressed and likely fragment during its passage through the water column. We also noted above that our own method of calculating the experimental velocities at the basement rock may become unreliable at greater water depths, due to the expected dispersal and fragmentation of the projectile. It can be seen that as the water depth increases, the velocity of the projectile at the ocean-basement rock interface is decreased by progressively greater amounts with increasing water depth. Even for a water depth of just 1 mm the water column has a small influence on the projectile's velocity, decreasing it to between 84% and 90% of its original value (where the range represents the three different methods used). For a water depth of 5 mm where there is still a crater produced in the granite, the velocity is decreased to 26–32% of its original value (or 43% as calculated with the SSD). For deep water impacts the remaining velocity in the projectile (0–2% of original value, or 19% as calculated with the SSD) is not significant to produce cratering.

DISCUSSION AND CONCLUSION

The effect of projectile parameters on crater morphology and the fate of the projectile for different water depths have been investigated at a laboratory scale. In terms of crater morphology, we initially compared previously published results (Baldwin et al. 2007) describing impacts into saturated and unsaturated sandstone with an overlying water layer of varying depth with data presented here for impacts into granite with an overlying water layer. We find that the depths and diameters of the resulting craters decay linearly for impacts into sandstone but exponentially for granite. While the impact conditions and analytical techniques were identical for the two sets of the experiments, the main difference between these two materials are their intrinsic properties such as strength, density and porosity, the effects of which cannot be separated. We also find a difference in the water depth to projectile diameter ratio required to prevent cratering for the two different basement rocks; as ~10 for granite, and 11.6 ± 0.5 and 12.7 ± 0.6 for unsaturated and saturated sandstone, respectively. Since sandstone is weaker than granite, it is a natural conclusion that the weaker material requires more water to protect it from cratering, a result also supported by the work of Gault and Sonett (1982) who showed the H/d to be ~20 for unconsolidated sand targets. Indeed, in a separate experimental study we found the strength of our unsaturated and saturated sandstone to be 90 MPa and 43 MPa, respectively (Baldwin et al. 2007),

Table 7. Projectile velocity at the basement rock as calculated from the experiments, numerical models and SSD. The initial impact velocity is the velocity recorded by the light gas gun and is accurate to 1%. All experiments used 1 mm diameter stainless steel 420 projectiles, impacting into varying depth water layers overlaying a granite basement rock.

		Projectile velocity at basement rock (km s^{-1})		
Water depth (mm)	Initial impact velocity (km s^{-1})	Determined via experiments	Determined using AUTODYN	Calculated via SSD approximation
0	5.30	5.30	5.00	5.00
1	5.32	4.48	4.50	4.22
3	5.23	2.71	3.18	3.01
5	5.49	1.72	1.28	2.15
7.5	5.15	0.52	0.33	1.41
10	5.28	0	0.10	0.93

while the strength of granite is 344 MPa (Saito et al. 2006). For planetary-scale impacts, Artemieva and Shuvalov (2002) show that oceanic depths twice that of the projectile diameter begin to influence crater formation, while for water depths four times the projectile diameter a sea-floor crater is almost non-existent, for typical planetary impact velocities of 15–40 km s^{-1}.

We also investigate other factors that can influence cratering: impact velocity and impact angle. For water depths between 0 and 5 times the projectile diameter, increasing impact velocity was found to increase crater dimensions exponentially, but this increase tapered off for higher velocities. Regardless of velocity, crater dimensions were reduced for increasing amounts of water. While investigating the effect of impact angles on crater formation, we maintained a constant water column depth and found that crater dimensions decreased linearly as the impact angle increased from the vertical. When considering the decay in velocity in the projectile between impact with the water column and arrival at the pre-impact basement rock, the velocity is found to be reduced to 26–32% its original value, when considering an impact into a water depth five times the projectile diameter, and almost slowed completely for deep water events. The velocity decay in lab experiments and lab scale AUTODYN models agree well and show that velocity decay occurs exponentially.

It has been previously demonstrated that a significant amount of projectile material can survive laboratory scale impacts (e.g., Gault and Sonett 1982; Milner et al. 2006), and here we found that for stainless steel projectiles impacting into deep water at 5 km s^{-1}, as much as 30% of the original mass of the projectile was found to survive in planar impact events, and up to 60% survives an oblique impact event, with the optimum mass of surviving fragments found for angles of 30–35 degrees from the vertical. The fate of the projectile during a marine impact event is highly dependent upon the peak pressures the projectile experiences at the top of the water column where the kinetic energy of the impact event is first deposited, and second, should the projectile remain largely intact as it traverses the water layer, at the ocean-target interface. In turn, the peak pressure experienced in the impact is dependent upon the vertical component of the projectile velocity (Pierazzo and Melosh 2000b), with more oblique impacts resulting in a lower peak pressure experienced by the bulk of the projectile, which enhances survivability. Calculations of the shock pressures for our laboratory experiments suggest that not all the projectile reaches incipient melting pressures, offering an explanation as to how so much material is retrieved in the lab after impact.

At planetary scale an ocean will also slow an incoming asteroid, although the maximum size of an asteroid that can successful pass through the Earth's atmosphere without disruption will be 200 m in diameter at the top of the ocean (Chyba et al 1993). Asteroids comparable to the depth of Earth's oceans and greater (an average of 3.6 km, O'Keefe and Ahrens 1982) will not see the effects of an ocean. However, for a simulated 45 degree impact at 20 km s^{-1} of a 1 km diameter asteroid into an ocean 1 or 2 km deep, the projectile is seen to fragment before reaching the ocean floor, with some fragments separating very early and moving upward with excavated water (Artemieva and Shuvalov 2002), suggesting that projectile survivability is enhanced with oblique angle at planetary scale as well as in the lab.

For the Earth, of the few impact craters known to have occurred into water, the only known deep sea impact event to date is the 2.2 Ma old Eltanin structure located in the Bellingshausen Sea (Gersonde et al. 1997; Gersonde and Kyte 2001; Shuvalov and Trubetskaya 2007) which is characterized by a zone of chaotically mixed sediments, most likely originating from impact-induced turbulent water currents (Wünnemann and Lange 2002). Present observations do not allow identification of an impact crater on the ocean bottom. The evidence for the event being of impact origin was the discovery of an iridium anomaly in ocean floor deposits, with the maximum concentrations found in vesicular fragments that were interpreted to have formed by melting of the projectile (Kyte et al. 1981; Kyte 2002). Meteoritic material was also found in three locations spaced 500 km apart; unmelted fragments of the impactor of less than 2 cm in size were also recovered. It has also been reported that 25 cm fragments of meteoritic material have been recovered from the continental impact of Morokweng crater in South Africa (Maier et al. 2006), suggesting that material can survive not only in marine impacts but perhaps also in continental impacts as well.

Acknowledgments—We thank Ian Crawford for his helpful comments and support, and Mike Cole for operating the University of Kent's two-stage light gas gun. We also thank our reviewers Natalia Artemieva and Jens Ormö, and associate editor Elisabetta Pierazzo for their thorough reviews and suggestions, which have significantly improved the quality of the paper.

Editorial Handling—Dr. Elisabetta Pierazzo

REFERENCES

Artemieva N. A. and Shuvalov V. V. 2002. Shock metamorphism on the ocean floor (numerical simulations). *Deep Sea Research II* 49:959–968.

Allen P. J. and Stewart S. A. 2003. Silverpit: The morphology of a terrestrial multi-ringed impact structure (abstract #1351). 34th Lunar and Planetary Science Conference. CD-ROM.

AUTODYN Century Dynamics Limited, Suite 1, 3 Horsham Gates, North Street, Horsham, West Sussex, RH13 5PJ England; www.ansys.com.

Baldwin E. C., Milner D. J., Burchell M. J., and Crawford I. A. 2007. Influence of target saturation, porosity and an overlying water layer on crater morphologies in sandstone; Implications for scaling laws and projectile survivability. *Meteoritics & Planetary Science* 42:1–11.

Burchell M. J., Cole M. J., McDonnell J. A. M., and Zarnecki J. C. 1999. Hypervelocity impact studies using the 2MV Van der Graff accelerator and two stage light gas gun of the University of Kent at Canterbury. *Measurements Science and Technology* 10:41–50.

Burchell M. J., Mann J. R., and Bunch A. W. 2004. Survival of bacteria and spores under extreme pressures. *Monthly Notices of the Royal Astronomical Society* 352:1273–1278.

Burchell M. J. and Whitehorn L. 2003. Oblique incidence hypervelocity impacts on rock. *Monthly Notices of the Royal Astronomical Society* 341:192–198.

Chyba C. F., Thomas P. J., and Zahnle K. J. 1993. The 1908 Tunguska explosion: Atmospheric disruption of a stony asteroid. *Nature* 361:40–44.

Crawford I. A., Baldwin E. C., Taylor E. A., Bailey J., and Tsembelis K. 2008. On the survivability of terrestrial meteorites on the Moon. *Astrobiology* 8:242–252.

Dypvik H. and Jansa L. F. 2003. Sedimentary signatures and process during marine bolide impacts: A review. *Sedimentary Geology* 161:309–337.

Dypvik H., Ferrell R. E., and Sandbakken P. T. 2003. The clay mineralogy of sediments related to the marine Mjølnir impact crater. *Meteoritics & Planetary Science* 38:1437–1450.

Gault D. E. and Sonett C. P. 1982. Laboratory simulation of pelagic asteroid impact: Atmospheric injection, benthic topography, and the surface wave radiation field. In *Geological implications of impacts of large asteroids and comets on the Earth,* edited by Silver L. T. and Schultz P. H. GSA Special Paper 190. Boulder: Geological Society of America. pp. 69–92.

Gersonde R., Kyte F., Bleil U., Diekmann B., Flores J., Gohl K., Grahl G., Hagen R., Kuhn G., Sierros F., Völker D., Abelmann A., and Bostwick J. 1997. Geological record and reconstruction of the late Pilocene impact of the Eltanin asteroid in the Southern Ocean. *Nature* 390:357–363.

Gersonde R. and Deutsch A. 2000. New field of impact research looks to the ocean. *Eos* 81:221–232.

Gersonde R. and Kyte F. T. 2001. Exploration of the Eltanin impact area (Bellingshausen Sea): Expedition ANT XV1115a. *Meteoritics & Planetary Science* 36:A64.

Gersonde R., Deutsch A., Ivanov B. A., and Kyte F. T. 2002. Oceanic impacts—a growing field of fundamental geoscience. *Deep Sea Research II* 49:951–957.

Housen K. R. and Holsapple K. A. 1999. Scale effects in strength-dominated collisions of rocky asteroids. *Icarus* 142:21–33.

Kyte F. T., Zhou Z., and Wasson J. T. 1981. High noble metal concentrations in a late Pliocene sediment. *Nature* 292:417–420.

Kyte F. T. 2002. Unmelted meteoritic debris collected from Eltanin ejecta in polarstern cores from expedition ANT XII/4. *Deep Sea Research II* 49:1,063–1,071.

Maier W. D., Andreoli M. A. G, McDonald I., Higgins M. D., Boyce A. J., Shukolyukov A., Lugmair G. W., Aswell L. D., Graser P., Ripley E. M., and Hart R. J. 2006. Discovery of a 25-cm asteroid clast in the giant Morokweng impact crater, South Africa. *Nature* 441:203–206.

Melosh H. J. 1989. *Impact cratering: A geologic process*. New York: Oxford University Press. 245 p.

Milner D. J., Burchell M. J., Creighton J. A., and Parnell J. 2006. Oceanic hypervelocity impact events: A viable mechanism for successful panspermia? *International Journal of Astrobiology* 5:261–267.

Milner D. J. 2007. Simulations of oceanic hypervelocity impact events. Ph.D. thesis, University of Kent. Canterbury, UK. 236 p.

Mizutani H., Takagi Y., and Kawakami S. I. 1990. New scaling laws on impact fragmentation. *Icarus* 87:307–326.

O'Keefe J. D. and Ahrens T. J. 1981. The interaction of the Cretaceous/Tertiary extinction bolide with the atmosphere, ocean and solid Earth. GSA Special Paper 190. Geological Society of America, pp. 103–120.

Ormö J. and Lindstrom M. 2000. When a cosmic impact strikes the seabed. *Geological Magazine* 13:767–780.

Ormö J., Shuvalov V. V., and Lindström M. 2002. Numerical modeling for target water depth estimation of marine-target impact craters. *Journal of Geophysical Research Earth* 107, doi: 10.1029/2002JE001865.

Pierazzo E. and Melosh H. 2000a. Melt production in oblique impacts. *Icarus* 145:252–261.

Pierazzo E. and Melosh H. 2000b. Hydrocode modeling of oblique impacts: The fate of the projectile. *Meteoritics & Planetary Science* 35:117–130.

Saito T., Kaiho K., Abe A., Katayama M., and Takayama K. 2006. Numerical simulations of hypervelocity impact of asteroid/comet on the Earth. *International Journal of Impact Engineering* 33:713–722.

Shoemaker E. M. 1962. Interpretation of the lunar craters. In *Physics and astronomy of the Moon*, edited by Kopal Z. pp. 283–359.

Shrine N. R. G., Burchell M. J., and Grey I. D. S. 2002. Velocity scaling of impact craters in water ice over the range of 1–7.3 km s^{-1}. *Icarus* 155:475–485.

Shuvalov V. V. and Trubetskaya I. A. 2007. Numerical modeling of the formation of the Eltanin submarine impact structure. *Solar System Research* 41:56–64.

Tsikalas F., Gudlaugsson S. T., Faleide J. I., and Eldholm O. 1999. Mjølnir structure, Barents Sea: A marine impact crater laboratory. GSA Special Paper 339. Boulder: Geological Society of America. pp. 193–204.

Wünnemann K. and Lange M. A. 2002. Numerical modeling of impact-induced modifications of the deep-sea floor. *Deep Sea Research II* 49:969–981.